On the sound field of an oscillating disk in a finite open and closed circular baffle

Tim Mellow
Nokia UK Ltd., Farnborough, Hants GU14 0NG, England

Leo Kärkkäinen
Nokia Research Center, Helsinki, Finland

(Received 20 December 2004; revised 16 May 2005; accepted 27 June 2005)

Equations describing the radiation characteristics of a rigid disk in a finite open baffle are derived using a method similar to that used by Streng for a circular membrane based upon the dipole part of the Kirchhoff–Helmholtz boundary integral formula. In this case, however, a power series solution to the radiation integral is derived in order to eliminate the need for numerical integration. Hence, a set of simultaneous equations is obtained by simply equating the coefficients of the power series, which leads to two mathematical functions, one real and one imaginary, that can be applied to any radial velocity distribution. This provides an alternative method to obtain the sound scattered by a disk or the complementary hole in an infinite resilient screen according to Babinet's principle. Using the principle of superposition (or Gutin concept), it is shown how the sound radiation characteristics of a disk radiating from just one side can be obtained by combining the radiation field of a disk in a finite baffle with that of a disk in an infinite baffle. This one-sided radiator may be interpreted as a disk in a thin, circular enclosure. [DOI: 10.1121/1.2000828]

PACS number(s): 43.20.Rz, 43.20.Tb, 43.20.Fn, 43.20.Wd [LLT] Pages: 1311–1325

I. INTRODUCTION

The radiation characteristics of elementary sources are invaluable in providing lumped parameters for acoustics models based upon equivalent electrical circuits. Furthermore, they serve an important educational purpose in illustrating fundamental radiation and diffraction theory. They may also be used to provide benchmarks for boundary or finite element modeling (BEM/FEM). This can provide us with much information about the required element size and what kind of meshing geometry to use.

In addition to describing the radiation characteristics of a disk in an open or closed circular baffle, a more general aim of this paper is to present a simple unified approach to the problem of flat, axially symmetric sound sources based upon the Green's function in cylindrical coordinates and the Kirchhoff–Helmholtz boundary integral formula.[1] The latter is a general equation that describes the spatial distribution of the pressure within and on the surface bounding an acoustic medium. However, in the case of surfaces radiating into free space, the volume integral term can be omitted and the Green's function for an unbounded medium $g(\mathbf{r}|\mathbf{r}_0)$ is used so that the pressure distribution is described by

$$\tilde{p}(\mathbf{r}) = \int\int g(\mathbf{r}|\mathbf{r}_0)\frac{\partial}{\partial n_0}\tilde{p}(\mathbf{r}_0) - \tilde{p}(\mathbf{r}_0)\frac{\partial}{\partial n_0}g(\mathbf{r}|\mathbf{r}_0)dS_0, \quad (1)$$

where the first term (or *monopole* part) is the integral of the inward-pointed normal gradient of the boundary values of $p(\mathbf{r}_0)$ and $g(\mathbf{r}|\mathbf{r}_0)$ over the surface, and the second term (or *dipole* part) is the integral of the boundary values of $p(\mathbf{r}_0)$ and the inward-pointed normal gradient of $g(\mathbf{r}|\mathbf{r}_0)$ over the surface.

Many of the classical analytical results reproduced during the course of this paper are best known through the works of Beranek[2] and Olson.[3] Fifty years ago, it must have been a formidable task calculating these results without the benefits of modern computing power. Even today, the task of reproducing the results of the original papers,[4,5] from which they were derived, is perhaps not so trivial unless the reader is well versed in the mathematical methods used. Hence, it is useful to derive a compact set of equations suitable for modern computer applications. Bouwkamp[6] and Spence[7] independently derived the first rigorous solutions to the problem of the freely suspended disk using iterative methods based upon oblate spheroidal wave functions, while Meixner and Fritze[8] calculated its near-field pressure response. Nimura and Watanabe[9] calculated the radiation impedance and directivity of a rigid disk in a finite circular open baffle for lower values of ka. Pachner[10] described a calculation method using spherical Bessel and Legendre functions and used the superposition of fields, although no results were presented. Crane[11] calculated the radiation impedance of a circular piston in a closed circular baffle directly by applying the boundary conditions of a sound field resulting from the superposition of a disk in a finite open baffle upon a disk in an infinite baffle. In theory, it should be possible to extract the open baffle impedance from these results simply by doubling them and then subtracting the infinite baffle impedance. However, given the approximate nature of this calculation method and the fact that the real open baffle impedance is so small at low frequencies, the result is inevitably wildly inaccurate. In the last few decades, there has been much interest in time-domain techniques.

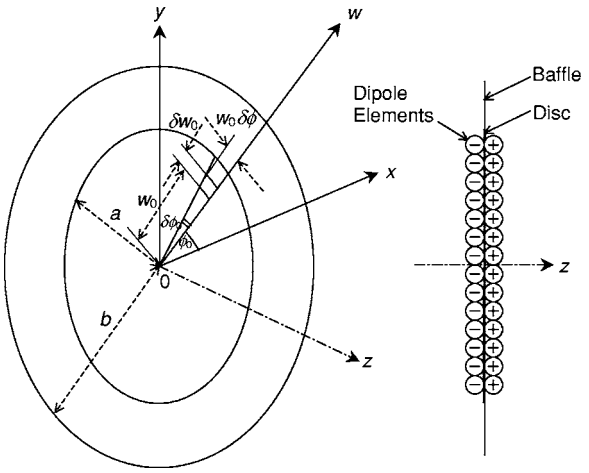

FIG. 1. Rigid disk in a finite open-back circular baffle.

Previously, one of the present authors[12] has used the least mean square (LMS) algorithm to tackle this problem, but found it to be numerically unsatisfactory for larger baffle sizes. Instead, the velocity of the radiator and its baffle is described, in this paper, by a step function using a Bessel function series, which produces a membrane-like expression. This allows a set of simultaneous equations to be obtained by simply equating the coefficients of the power series.

II. RIGID DISK IN A FINITE OPEN-BACK CIRCULAR BAFFLE

A. Boundary conditions

The disk shown in Fig. 1 lies in the xy plane, with its center at the origin and oscillates in the z direction with velocity $\tilde{u}_0$, thus radiating sound from both sides. The radius of the disk is a and it is assumed to be infinitesimally thin. It is surrounded by an infinitesimally thin circular baffle, the inner and outer radii of which are a and b, respectively. If $b=a$, the problem reduces to that of a *rigid disk in free space*. The area of each surface element is given by

$$\delta S_0 = w_0 \delta w_0 \delta \phi_0. \tag{2}$$

The pressure field on one side of the xy plane is the symmetrical "negative" of that on the other, so that

$$p(w,z) = -p(w,-z). \tag{3}$$

Consequently, there is a Dirichlet boundary condition in the plane of the disk where these equal and opposite fields meet.

$$p(w,0) = 0, \quad b < w \leqslant \infty \tag{4}$$

On the front and rear surfaces of the baffle, there is a Neumann boundary condition

$$\frac{\partial}{\partial z}\tilde{p}(w,z)|_{z=0\pm} = 0, \quad a < w \leqslant b. \tag{5}$$

Also, on the front and rear surfaces of the disk, there is the coupling condition

$$\frac{\partial}{\partial z}\tilde{p}(w,z)|_{z=0\pm} = -ik\rho c\tilde{u}_0(w), \quad 0 \leqslant w \leqslant a \tag{6}$$

where ρ is the density of air or any other surrounding medium, and c is the speed of sound in that medium. The annotation $\tilde{}$ denotes a harmonically time-varying quantity where we have suppressed the term $e^{i\omega t}$. In order to tackle this problem, we shall use the second term or *dipole* surface integral part of Eq. (1). However, some prior expression for the frontal surface pressure distribution $\tilde{p}_+(w_0)$ is needed. Also, because the disk can radiate from both sides, the rear surface pressure distribution $\tilde{p}_-(w_0)$ must be included too, where $\tilde{p}_+(w_0) = -\tilde{p}_-(w_0)$. Streng[13,14] showed that the surface pressure distribution for any flat, axially symmetric unbaffled source (or sink), based upon Bouwkamp's solution[6] to the free-space wave equation in oblate spheroidal coordinates, could be written as

$$\tilde{p}_+(w_0) = -\tilde{p}_-(w_0) = \sum_{m=0}^{\infty} \tilde{A}_m \left(1 - \frac{w_0^2}{b^2}\right)^{m+(1/2)}. \tag{7}$$

where $\tilde{A}_m$ are the as yet unknown power series coefficients.

B. Solution of the free-space wave equation

The pressure distribution, in accordance with the Huygens–Fresnel principle, is given by the second term or *dipole* part of Eq. (1) written in cylindrical coordinates as follows:

$$\tilde{p}(w,z) = -\int_0^{2\pi}\int_0^b (\tilde{p}_+(w_0) - \tilde{p}_-(w_0)) \times \frac{\partial}{\partial z_0} g(w,z|w_0,z_0)|_{z_0=0+} w_0 \, dw_0 \, d\phi_0, \tag{8}$$

where the Green's function $g(w|w_0)$ is the solution to the following free-space wave equation in the presence of a monopole point source located at (w_0,z_0) on the surface of the disk:

$$(\nabla^2 + k^2) g(w,z|w_0,z_0) = -\delta(w - w_0, z - z_0), \tag{9}$$

where

$$\nabla^2 = \frac{\partial^2}{\partial w^2} + \frac{1}{w}\frac{\partial}{\partial w} + \frac{\partial^2}{\partial z^2}, \tag{10}$$

$$k = \frac{2\pi}{\lambda} = \frac{\omega}{c}. \tag{11}$$

However, the pressure produced at each point (w,z) in space by each dipole element is defined in the integral of Eq. (8) by the product of the surface pressure, the inward-pointed normal gradient of the Green's function, and the area of each element given by Eq. (2). A solution to Eq. (9) is the free-space Green's function in cylindrical coordinates,[1] also known as the Lamb or Sommerfeld integral, which is given by

$$g(w,z|w_0,z_0) = \frac{i}{4\pi}\int_0^\infty J_0(\mu w)J_0(\mu w_0)\frac{\mu}{\sigma}e^{-i\sigma|z-z_0|}d\mu, \tag{12}$$

where

$$\sigma = \sqrt{k^2-\mu^2}. \tag{13}$$

Due to axial symmetry, only the zeroth term of the original power series is shown in Eq. (12). The normal gradient of the Green's function at the surface is given by

$$\frac{\partial}{\partial z_0} g(w,z|w_0,z_0)|_{z_0=0+} = \frac{1}{4\pi}\int_0^\infty J_0(\mu w)J_0(\mu w_0)\mu e^{-i\sigma z}d\mu. \tag{14}$$

Inserting this together with Eq. (7) in Eq. (8) and integrating over the surface of the disk and its baffle yields

$$\tilde{p}(w,z) = -b\sum_{m=0}^{\infty}\tilde{A}_m 2^{m+(1/2)}\Gamma\left(m+\frac{3}{2}\right)\int_0^\infty\left(\frac{1}{\mu b}\right)^{m+(1/2)} \times J_{m+(3/2)}(\mu b)J_0(\mu w)e^{-i\sigma z}d\mu, \tag{15}$$

where the following identity[15] has been used:

$$\int_0^a w_0\left(1-\frac{w_0^2}{b^2}\right)^{m+(1/2)}J_0(\mu w_0)dw_0 = b^2\int_0^1 t(1-t^2)^{m+(1/2)}J_0(\mu b t)dt = b^2 2^{m+(1/2)}\Gamma\left(m+\frac{3}{2}\right)\left(\frac{1}{\mu b}\right)^{m+(3/2)}J_{m+(3/2)}(\mu b), \tag{16}$$

where $t=w_0/b$. Applying the boundary conditions of Eq. (5) and Eq. (6) leads to

$$\frac{\partial}{\partial z}\tilde{p}(w,z)|_{z=0\pm} = ib\sum_{m=0}^{\infty}\tilde{A}_m 2^{m+(1/2)}\Gamma\left(m+\frac{3}{2}\right)\int_0^\infty\left(\frac{1}{\mu b}\right)^{m+(1/2)} \times J_{m+(3/2)}(\mu b)J_0(\mu w)\sigma d\mu = -ik\rho c\tilde{u}_0\Phi(w), \tag{17}$$

where

$$\Phi(w) = \begin{cases} 1, & 0 \leqslant w \leqslant a, \\ 0, & a < w \leqslant b. \end{cases} \tag{18}$$

C. Series representation of the velocity distribution

Let the Bessel series have the form

$$\Phi(w) = \sum_{n=1}^{\infty} a_n J_0(j_{0n}w/b), \tag{19}$$

where j_{0n} is the nth zero of J_0 such that $J_0(j_{0n})=0$. Multiplication of Eq. (19) by the normalizing function $J_0(j_{0m}w/b)$ and integration over w gives

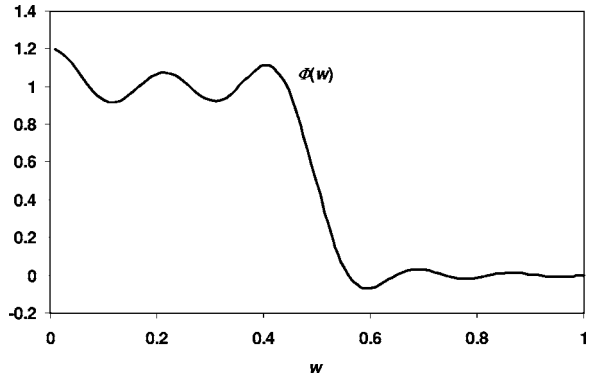

FIG. 2. Bessel series representation of the surface velocity distribution.

$$\int_0^b \Phi(w)J_0(j_{0m}w/b)w\,dw = \int_0^a J_0(j_{0m}w/b)w\,dw = \sum_{n=1}^{\infty}a_n\int_0^b J_0(j_{0n}w/b)J_0(j_{0m}w/b)w\,dw. \tag{20}$$

Integrating over w yields

$$\frac{ab}{j_{0m}}J_1(j_{0m}a/b) = \frac{b^2}{2}\sum_{n=1}^{\infty}a_n\delta_{mn}J_1^2(j_{0n}), \tag{21}$$

where the following identities[15] have been employed:

$$\int_0^a J_0(j_{0m}w/b)w\,dw = \int_0^1 J_0(j_{0m}ay/b)y\,dy = abJ_1(j_{0m}a/b)/j_{0m}, \tag{22}$$

and

$$\int_0^1 J_0(\alpha x)J_0(\beta x)x\,dx = \begin{cases} 0, & \alpha\neq\beta, \\ J_1^2(\alpha)/2, & \alpha=\beta, \end{cases} \tag{23}$$

where $y=w/a$, $x=w/b$ and α, β are zeros of J_0. Hence

$$a_n = 2\frac{aJ_1(j_{0n}a/b)}{bj_{0n}J_1^2(j_{0n})}. \tag{24}$$

A series expansion[15] of $J_0(j_{0n}w/b)$ is given by

$$J_0(j_{0n}w/b) = \sum_{q=0}^{\infty}\frac{(-1)^q}{(q!)^2}\left(\frac{j_{0n}}{2}\right)^{2q}\left(\frac{w}{b}\right)^{2q}. \tag{25}$$

Substituting Eq. (24) and Eq. (25) in Eq. (19) yields

$$\Phi(w) = \frac{a}{b}\sum_{n=1}^{N}\sum_{q=0}^{Q}\frac{(-1)^q J_1(j_{0n}a/b)}{(q!)^2J_1^2(j_{0n})}\left(\frac{j_{0n}}{2}\right)^{2q-1}\left(\frac{w}{b}\right)^{2q}, \tag{26}$$

where both infinite power series limits have been truncated. The result is plotted in Fig. 2 for $a=\frac{1}{2}$, $b=1$, $N=10$, and $Q=50$.

D. Formulation of the coupled problem

Equation (17) can be written more simply as

$$\sum_{m=0}^{\infty} \tau_m I_m(w,k) = -\Phi(w), \tag{27}$$

which needs to be solved for the normalized power series coefficients τ_m, where

$$\tau_m = \frac{\tilde{A}_m}{(m+3/2)kb\rho c\tilde{u}_0}, \tag{28}$$

and

$$I_m(w,k) = I_{mR}(w,k) + iI_{mI}(w,k), \tag{29}$$

where the real part of the integral in Eq. (29) is given by

$$I_{mR}(w,k) = b^2\Gamma\left(m+\frac{5}{2}\right)\int_0^k \left(\frac{2}{\mu b}\right)^{m+(1/2)} \times \sqrt{k^2-\mu^2}J_{m+(3/2)}(\mu b)J_0(\mu w)d\mu, \tag{30}$$

and the imaginary part is given by

$$I_{mI}(w,k) = b^2\Gamma\left(m+\frac{5}{2}\right)\int_k^{\infty} \left(\frac{2}{\mu b}\right)^{m+(1/2)} \times \sqrt{\mu^2-k^2}J_{m+(3/2)}(\mu b)J_0(\mu w)d\mu. \tag{31}$$

E. Solution of the real integral

Substitution of $\mu = k\sin\vartheta$ in Eq. (30) gives

$$I_{mR}(w,k) = 4\Gamma\left(m+\frac{5}{2}\right)\left(\frac{2}{kb}\right)^{m-(3/2)}\int_0^{\pi/2}\frac{\cos^2\vartheta}{(\sin\vartheta)^{m+1/2}} \times J_0(kw\sin\vartheta)J_{m+(3/2)}(kb\sin\vartheta)d\vartheta. \tag{32}$$

A series expansion[15] of $J_{m+3/2}(kb\sin\vartheta)$ is given by

$$J_{m+(3/2)}(kb\sin\vartheta) = \sum_{q=0}^{Q}\left(\frac{kb}{2}\right)^{2q+m+(3/2)}\frac{(-1)^q(\sin\vartheta)^{2q+m+3/2}}{q!\Gamma(q+m+5/2)}. \tag{33}$$

Replacing j_{0n}/b in Eq. (25) with $k\sin\vartheta$, and substituting this together with Eq. (33) in Eq. (32) gives

$$I_{mR}(w,k) = 4\sum_{q=0}^{Q}\sum_{r=0}^{R}\frac{(-1)^{q+r}\Gamma(m+5/2)}{(q!)^2r!\Gamma(r+m+5/2)}\left(\frac{w}{b}\right)^{2q} \times \left(\frac{kb}{2}\right)^{2(q+r)+3}\int_0^{\pi/2}\cos^2\vartheta(\sin\vartheta)^{2(q+r)+1}d\vartheta. \tag{34}$$

Solution of the integral in Eq. (34) is enabled by use of the following identity:[16]

$$\int_0^{\pi/2}\cos^2\vartheta(\sin\vartheta)^{2(q+r)+1}d\vartheta = \frac{\sqrt{\pi}\Gamma(q+r+1)}{4\Gamma(q+r+5/2)}. \tag{35}$$

Evaluating the integral over ϑ yields

$$I_{mR}(w,k) = \sum_{q=0}^{Q}\sum_{r=0}^{R}\frac{\sqrt{\pi}(-1)^{q+r}\Gamma(m+5/2)\Gamma(q+r+1)}{(q!)^2r!\Gamma(r+m+5/2)\Gamma(q+r+5/2)} \times \left(\frac{kb}{2}\right)^{2(q+r)+3}\left(\frac{w}{b}\right)^{2q}. \tag{36}$$

F. Solution of the imaginary integral

In order to change the infinite limit of Eq. (31) to a finite one, Streng[13] replaced the Bessel function $J_{q+3/2}$ with Hankel functions $H^{(1)}_{q+3/2}+H^{(2)}_{q+3/2}$. By applying contour integration theory, together with the substitution $\mu = ke^{i\vartheta}$, he showed that the imaginary integral Eq. (31) could be expressed as

$$I_{mI}(w,k) = \Re\left(4i\left(\frac{2}{kb}\right)^{m-(3/2)}\Gamma\left(m+\frac{5}{2}\right) \times \int_0^{\pi/2} e^{i[(1/2)-m]\vartheta}\sqrt{e^{2i\vartheta}-1}J_0(kwe^{i\vartheta}) \times \{J_{m+(3/2)}(kbe^{i\vartheta}) + iY_{m+(3/2)}(kbe^{i\vartheta})\}d\vartheta\right). \tag{37}$$

A series expansion[15] of the Neumann function is given by

$$Y_{m+(3/2)}(kbe^{i\vartheta}) = \sum_{q=0}^{Q}\left(\frac{kb}{2}\right)^{2q-m-(3/2)}\frac{(-1)^{q+m}e^{i\vartheta(2q-m-3/2)}}{q!\Gamma(q-m-1/2)}. \tag{38}$$

Replacing j_{0n}/b in Eq. (25) and $k\sin\vartheta$ in Eq. (33) with $ke^{i\vartheta}$, and substituting these together with Eq. (38) in Eq. (37) gives

$$I_{mI}(w,k) = -4\sum_{q=0}^{Q}\sum_{r=0}^{R}\Re\left(\frac{(-1)^{q+r}\Gamma(m+5/2)}{(q!)^2r!\Gamma(r+m+5/2)}\left(\frac{w}{b}\right)^{2q} \times \left(\frac{kb}{2}\right)^{2(q+r)+3} i\int_0^{\pi/2}\sqrt{e^{2i\vartheta}-1}e^{2i\vartheta(q+r+1)}d\vartheta - \frac{(-1)^{q+r+m}\Gamma(m+5/2)}{(q!)^2r!\Gamma(r-m-1/2)}\left(\frac{w}{b}\right)^{2q}\left(\frac{kb}{2}\right)^{2(q+r-m)} \times \int_0^{\pi/2}\sqrt{e^{2i\vartheta}-1}e^{2i\vartheta[q+r-m-(1/2)]}d\vartheta\right). \tag{39}$$

Solution of the integrals in Eq. (37) is enabled by use of the following identity:[16]

$$\int_0^{\pi/2}\sqrt{e^{2i\vartheta}-1}e^{2i\gamma\vartheta}d\vartheta = \frac{1}{2\gamma}\left({}_2F_1\left(-\frac{1}{2},\gamma;\gamma+1;-1\right)e^{i\pi\gamma} - \frac{\sqrt{\pi}\Gamma(\gamma+1)}{2\Gamma(\gamma+3/2)}\right). \tag{40}$$

Evaluating the integrals over ϑ yields

$$I_{ml}(w,k) = 4\Gamma\left(m+\frac{5}{2}\right)\Re\left(\sum_{q=0}^{Q}\sum_{r=0}^{R} F_{\mathrm{Y}}(q,r,m)\left(\frac{kb}{2}\right)^{2(q+r-m)} \times \left(\frac{w}{b}\right)^{2q} - iF_{\mathrm{J}}(q,r,m)\left(\frac{kb}{2}\right)^{2(q+r)+3}\left(\frac{w}{b}\right)^{2q}\right), \tag{41}$$

where the subfunctions F_{Y} and F_{J} are given by

$$F_{\mathrm{Y}}(q,r,m) = (-1)^{q+r+m}\left(\frac{{}_2F_1(-1/2,\alpha;\alpha+1;-1)e^{i\pi\alpha}}{2\alpha(q!)^2 r!\Gamma(r-m-1/2)} - \frac{\sqrt{\pi}\Gamma(\alpha)}{4(q!)^2 r!\Gamma(r-m-1/2)\Gamma(\alpha+3/2)}\right), \tag{42}$$

$$F_{\mathrm{J}}(q,r,m) = (-1)^{q+r}\left(\frac{{}_2F_1(-1/2,\beta;\beta+1;-1)e^{i\pi\beta}}{2\beta(q!)^2 r!\Gamma(r+m+5/2)} - \frac{\sqrt{\pi}\Gamma(\beta)}{4(q!)^2 r!\Gamma(r+m+5/2)\Gamma(\beta+3/2)}\right), \tag{43}$$

where

$$\alpha = q+r-m-1/2, \tag{44}$$

$$\beta = q+r+1. \tag{45}$$

However, for integer values of q and r, $iF_{\mathrm{J}}(q,r,m)$ is purely imaginary and therefore makes no contribution to the real part of $I_{ml}(w,k)$. Similarly, the $e^{i\pi(q+r-m-1/2)}$ term of $F_{\mathrm{Y}}(q,r,m)$ is also purely imaginary and can therefore be excluded. Thus, the final result can be written

$$I_{ml}(w,k) = -\sum_{q=0}^{Q}\sum_{r=0}^{R}\frac{\sqrt{\pi}(-1)^{q+r+m}\Gamma(m+5/2)\Gamma(q+r-m-1/2)}{(q!^2 r!\Gamma(r-m-1/2)\Gamma(q+r-m+1)} \times\left(\frac{kb}{2}\right)^{2(q+r-m)}\left(\frac{w}{b}\right)^{2q}. \tag{46}$$

G. Calculation of the power series coefficients (final set of simultaneous equations)

Truncating the infinite power series in Eq. (27) to order M and equating the coefficients of $(w/b)^{2q}$ yields the final set of M simultaneous equations in τ_m as follows:

$$\sum_{m=0}^{M}({}_m\mathbf{B}_q(kb) - i\,{}_m\mathbf{S}_q(kb))\tau_m = -\Phi_q, \tag{47}$$

where $\mathbf{B}$ shall be named the *Bouwkamp* function as defined by

$${}_m\mathbf{B}_q(kb) = \sqrt{\pi}\sum_{r=0}^{M}\frac{(-1)^{q+r}\Gamma(m+5/2)\Gamma(q+r+1)}{r!(q!)^2\Gamma(r+m+5/2)\Gamma(q+r+5/2)} \times\left(\frac{kb}{2}\right)^{2(q+r)+3}, \tag{48}$$

and $\mathbf{S}$ shall be named the *Streng* function as defined by

$${}_m\mathbf{S}_q(kb) = \sqrt{\pi}\sum_{r=0}^{M}\frac{(-1)^{q+r+m}\Gamma(m+5/2)\Gamma(q+r-m-1/2)}{r!(q!)^2\Gamma(r-m-1/2)\Gamma(q+r-m+1)} \times\left(\frac{kb}{2}\right)^{2(q+r-m)}, \tag{49}$$

and

$$\Phi_q = \frac{a}{b}\sum_{n=1}^{N}\frac{(-1)^q J_1(j_{0n}a/b)}{(q!)^2 J_1^2(j_{0n})}\left(\frac{j_{0n}}{2}\right)^{2q-1}, \tag{50}$$

which is solved for $q=0,1,2,\ldots,M-1$, M. In the case of $b=a$, the problem reduces to that of *a rigid disk in free space*, in which case

$$\Phi_q = \delta_{q0}, \tag{51}$$

where δ_{q0} is the Kronecker delta function. In the case of $b=8a$, calculations were performed with $M=200$, $N=40$, and 140 digits of precision. These values were reduced in proportion to b/a for smaller baffle sizes.

H. Surface pressure

From Eq. (28), it follows that

$$\tilde{A}_m = \tau_m(m+3/2)kb\rho c\tilde{u}_0. \tag{52}$$

After substituting this in Eq. (7), the surface pressure can be written as

$$\tilde{p}_+(w_0) = kb\rho c\tilde{u}_0\sum_{m=0}^{M}\left(m+\frac{3}{2}\right)\tau_m\left(1-\frac{w_0^2}{b^2}\right)^{m+(1/2)}. \tag{53}$$

I. Radiation impedance

The total force $\tilde{F}$ acting upon the disk can be found by integrating the pressure from Eq. (53) over its surface on *both* sides as follows:

$$\tilde{F} = -\int_0^{2\pi}\int_0^a 2\tilde{p}_+(w_0)w_0\,dw_0\,d\phi_0 = -2\pi kb^3\rho c\tilde{u}_0\sum_{m=0}^{M}\tau_m\left\{1-\left(1-\frac{a^2}{b^2}\right)^{m+(3/2)}\right\}. \tag{54}$$

The acoustic radiation impedance z_{ar} is then given by

$$z_{ar} = \frac{\tilde{F}}{S\tilde{U}_0} = \frac{\tilde{F}}{S^2\tilde{u}_0} = \frac{2\rho c}{S}(R_{\mathrm{R}} + iX_{\mathrm{R}}), \tag{55}$$

where $\tilde{U}_0$ is the total volume velocity produced by the disk and S is the area of the disk given by $S=\pi a^2$. R_{R} is the normalized radiation *resistance* given by

$$R_{\mathrm{R}} = -kb\frac{b^2}{a^2}\sum_{m=0}^{M}\Re(\tau_m)\left\{1-\left(1-\frac{a^2}{b^2}\right)^{m+(3/2)}\right\}, \tag{56}$$

and X_{R} is the normalized radiation *reactance* given by

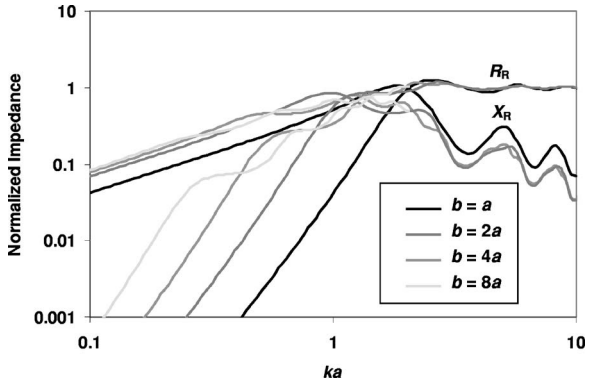

FIG. 3. Normalized radiation impedance of a disk in a finite open-back baffle.

$$X_{\mathrm{R}} = -kb\frac{b^2}{a^2}\sum_{m=0}^{M}\mathfrak{I}(\tau_m)\left\{1-\left(1-\frac{a^2}{b^2}\right)^{m+(3/2)}\right\}. \tag{57}$$

This result is plotted in Fig. 3. By using standard curve-fitting methods, the following asymptotic expressions can be written:

$$R_{\mathrm{R}} \approx 0.068\left(\frac{b^2}{a^2}-0.56\right)k^4a^4, \quad kb<0.5, \tag{58}$$

$$X_{\mathrm{R}} \approx \frac{8(3b-2a)}{3\pi(3b-a)}ka, \quad kb<0.5. \tag{59}$$

J. Near-field pressure response

Applying expression for $\tilde{A}_m$ in Eq. (52) to Eq. (15), the normalized near-field pressure can be written

$$\frac{\tilde{p}(w,z)}{\rho c\tilde{u}_0} = -kb^2\sum_{m=0}^{\infty}\tau_m\Gamma\left(m+\frac{5}{2}\right) \times\int_0^{\infty}\left(\frac{2}{\mu b}\right)^{m+(1/2)}J_{m+(3/2)}(\mu b)J_0(\mu w)e^{-i\sigma z}d\mu. \tag{60}$$

By substituting $\mu=kt$, Eq. (60) can be written

$$\frac{\tilde{p}(w,z)}{\rho c\tilde{u}_0} = -4\sum_{m=0}^{M}\tau_m\Gamma\left(m+\frac{5}{2}\right)\left(\frac{2}{kb}\right)^{m-(3/2)} \times\left(\int_0^1\frac{1}{t^{m+(1/2)}}e^{-ikz\sqrt{1-t^2}}J_{m+(3/2)}(kbt)J_0(kwt)dt + \int_1^{\infty}\frac{1}{t^{m+(1/2)}}e^{-kz\sqrt{t^2-1}}J_{m+(3/2)}(kbt)J_0(kwt)dt\right). \tag{61}$$

The infinite integral in Eq. (61) converges so rapidly that the infinite limit can be replaced with a finite value of say, 50, without significant loss of accuracy. The result is shown in Fig. 4 for $b=2a$ with various values of ka.

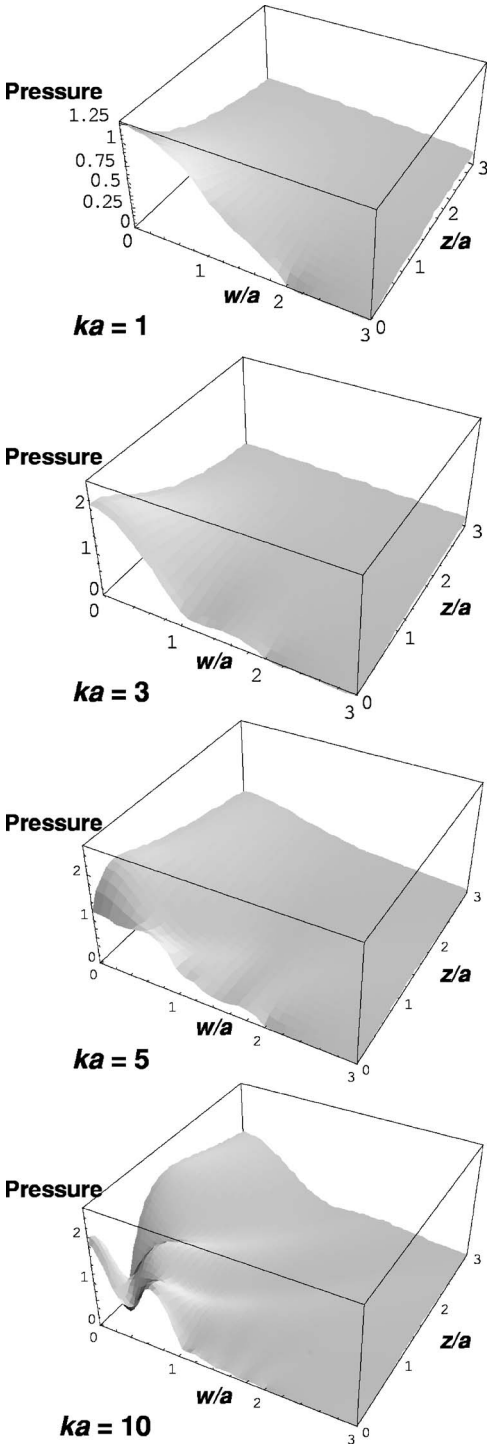

FIG. 4. Near-field pressure response of a disk in a finite open-back baffle with $b=2a$.

K. Far-field pressure response

In the case of the far-field response, it is more convenient to use spherical coordinates so that the far-field polar responses can be obtained directly. Rayleigh's far-field approximation[1] is ideal for this purpose

$$g(r,\theta,\phi|w_0,\phi_0,z_0) = \frac{1}{4\pi r}e^{-ik[r-w_0\sin\theta\cos(\phi-\phi_0)-z_0\cos\theta]}. \tag{62}$$

Again, the second term or *dipole* part of Eq. (1) is used, but this time in spherical coordinates

$$\tilde{p}(r,\theta,\phi) = -\int_0^{2\pi}\int_0^b (\tilde{p}_+(w_0) - \tilde{p}_-(w_0)) \times \frac{\partial}{\partial z_0} g(r,\theta,\phi|w_0,\phi_0,z_0)|_{z_0=0+} w_0\, dw_0\, d\phi_0. \tag{63}$$

However, it is necessary to find the surface normal gradient of the far-field Green's function given in Eq. (62)

$$\frac{\partial}{\partial z_0} g(r,\theta,\phi|w_0,\phi_0,z_0)|_{z_0=0+} = ik\cos\theta \frac{1}{4\pi r} e^{-ikr} \times e^{ikw_0 \sin\theta\cos(\phi-\phi_0)}. \tag{64}$$

As the disk is axially symmetric, any reference angle ϕ may be chosen in Eq. (64). Therefore, the problem can be simplified by letting $\phi=\pi/2$ so that $\cos(\phi-\phi_0)=\sin\phi_0$. Inserting Eq. (64) and Eq. (53) into Eq. (63) and integrating over the surface of the disk yields

$$\tilde{p}(r,\theta) = -ik\rho c S\tilde{u}_0 \frac{1}{2\pi r} e^{-ikr} D(\theta), \tag{65}$$

where S is the area of the disk, given by $S=\pi a^2$, and the following identities[15] have been used:

$$\frac{1}{2\pi}\int_0^{2\pi} e^{it\sin\phi_0} d\phi_0 = J_0(t), \tag{66}$$

where $t=kw_0\sin\theta$ together with Eq. (16), where $\mu = k\sin\theta$. The directivity function $D(\theta)$ is given by

$$D(\theta) = -kb\frac{b^2}{a^2}\cos\theta \sum_{m=0}^{M} \tau_m \Gamma\left(m+\frac{5}{2}\right)\left(\frac{2}{kb\sin\theta}\right)^{m+(3/2)} \times J_{m+(3/2)}(kb\sin\theta). \tag{67}$$

The on-axis pressure is evaluated using $\theta=0$ in Eq. (64) before inserting it into Eq. (63). This results in an integral that is similar to the one for the radiation impedance in equation Eq. (54). Hence

$$D(0) = -kb\frac{b^2}{a^2}\sum_{m=0}^{M}\tau_m. \tag{68}$$

It is worth noting that in the unbaffled case, where $b=a$, the on-axis response is simply defined by $D(0)=R_R+iX_R$. Again, using standard curve-fitting methods, the following asymptotic expression can be written:

$$D(0) \approx i0.66\left(\frac{b}{a}-0.3\right)ka, \quad kb<0.5. \tag{69}$$

The normalized on-axis response is shown in Fig. 5, where the normalized SPL is given by

$$\mathrm{SPL}_{\mathrm{Norm}} = 20\log_{10}|D(0)|. \tag{70}$$

The normalized directivity function $20\log_{10}(|D(\theta)|/|D(0)|)$ is plotted in Fig. 6 with $b=2a$ for various values of ka and in Fig. 7 with $ka=\pi/2$ for various values of b/a.

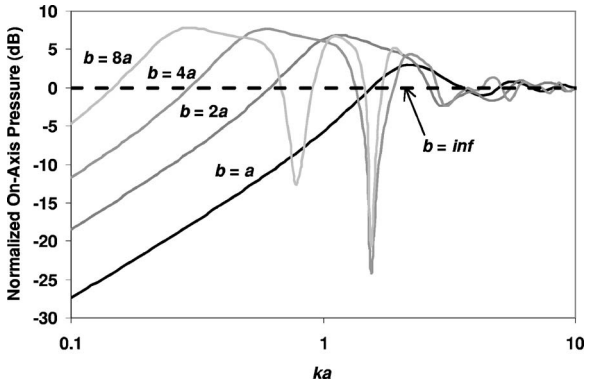

FIG. 5. Normalized far-field on-axis response of a disk in a finite open-back baffle with constant acceleration.

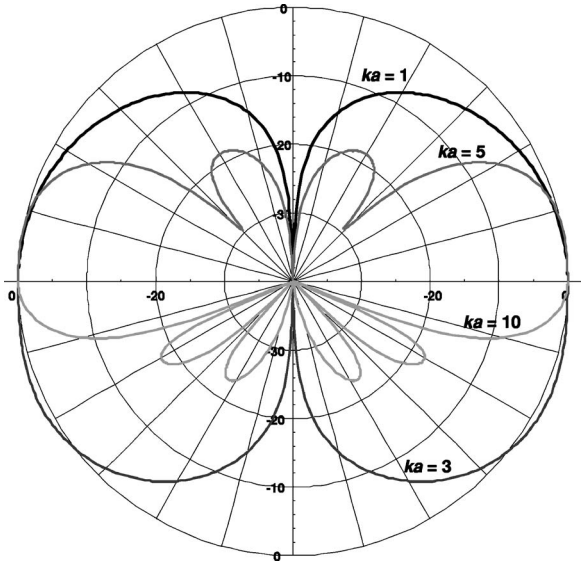

FIG. 6. Normalized far-field directivity function of a disk in a finite open-back baffle with $b=2a$.

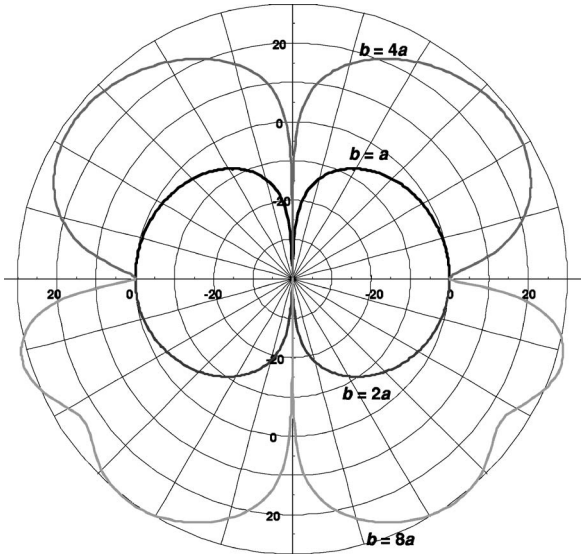

FIG. 7. Normalized far-field directivity function of a disk in a finite open-back baffle with $ka=\pi/2$.

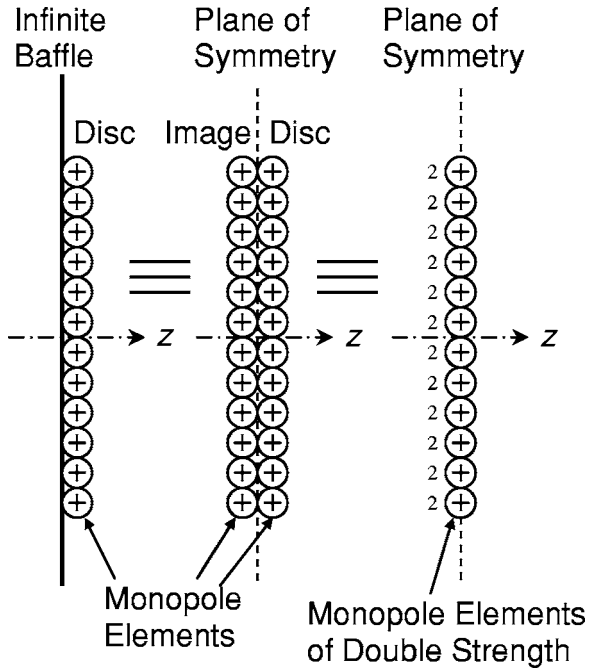

FIG. 8. Rigid disk in an infinite baffle.

III. RIGID DISK IN AN INFINITE BAFFLE

A. Boundary conditions

The original derivation of the radiation impedance by Lord Rayleigh[17] over 100 years ago used an ingenious coordinate system to simplify the problem. Stenzel[18] derived the near-field pressure response using the simple omnidirectional Green's function. Since equations describing the radiation characteristics of a disk in an infinite baffle are needed for Sec. IV, it is perhaps worth providing a brief review of King's method,[19] which is consistent with Sec. II as it uses the Green's function in cylindrical coordinates.

The disk shown in Fig. 1 is now mounted in an infinite baffle in the xy plane and oscillates in the z direction with a harmonically time-dependent velocity $\tilde{u}_0$. The area of each surface element is given by Eq. (2). However, the dipole elements are replaced with *monopole* elements as shown in Fig. 8. The monopole source elements and their images together form the disk source. Since they are coincident in the plane of the baffle, they combine to form elements of double strength. Hence, the disk in an infinite baffle can be modeled as a "breathing" disk in free space. It may also be considered as a pulsating sphere of the same radius compressed into the plane of the disk. Due to the symmetry of the pressure fields on either side of the baffle, there is the following Neumann boundary condition on its surface:

$$\frac{\partial}{\partial z}\,\tilde{p}(w,z)|_{z=0+} = 0, \quad a < w \leqslant \infty, \tag{71}$$

and on the surface of the disk there is the coupling condition

$$\frac{\partial}{\partial z}\,\tilde{p}(w,z)|_{z=0+} = -ik\rho c\tilde{u}_0, \quad 0 \leqslant w \leqslant a, \tag{72}$$

where ρ is the density of air or any other surrounding medium and c is the speed of sound in that medium.

B. Near-field pressure

The pressure distribution, in accordance with the Huygens–Fresnel principle, is given by the first term or *monopole* part of Eq. (1) taking into account the double-layer source

$$\tilde{p}(w,z) = 2\int_0^{2\pi}\int_0^a g(w,z|w_0,z_0) \times \frac{\partial}{\partial z_0}\,\tilde{p}(w_0,z_0)|_{z_0=0+} w_0\, dw_0\, d\phi_0. \tag{73}$$

Inserting the Green's function of Eq. (12), together with Eq. (72), into Eq. (73), while integrating over the surface of the disk yields

$$\frac{\tilde{p}(w,z)}{\rho c\tilde{u}_0} = -ka\int_0^\infty J_1(\mu a)J_0(\mu w)\frac{1}{\sigma}e^{-i\sigma z}d\mu, \tag{74}$$

where we have used Eq. (22) with $y=w_0/a$ and $\mu=j_{0m}/b$. By substituting $\mu=kt$, Eq. (74) can be written

$$\frac{\tilde{p}(w,z)}{\rho c\tilde{u}_0} = -ka\left(\int_0^1 \frac{1}{\sqrt{1-t^2}}e^{-ikz\sqrt{1-t^2}}J_1(kat)J_0(kwt)dt + i\int_1^\infty \frac{1}{\sqrt{t^2-1}}e^{-kz\sqrt{t^2-1}}J_1(kat)J_0(kwt)dt\right). \tag{75}$$

The infinite integral in Eq. (75) converges so rapidly that the infinite limit can be replaced with a finite value of, say, 50 without significant loss of accuracy. This result is shown in Fig. 9 for various values of ka.

C. Radiation impedance

The total force $\tilde{F}$ acting upon the disk can be found by integrating the pressure from Eq. (74) over its surface as follows:

$$\tilde{F} = -\int_0^{2\pi}\int_0^a \tilde{p}\,(w,z)|_{z=0+} w\, dw\, d\phi = 2\pi ka^2\rho c\tilde{u}_0 \times \left(\int_0^k \frac{J_1^2(\mu a)}{\mu\sqrt{k^2-\mu^2}}d\mu - i\int_k^\infty \frac{J_1^2(\mu a)}{\mu\sqrt{\mu^2-k^2}}d\mu\right), \tag{76}$$

where Eq. (22) has again been used. Using King's solutions[19] to the integrals over μ in Eq. (76) leads to the following expression for the acoustic radiation impedance:

$$z_{\mathrm{ar}} = \frac{\tilde{F}}{S\tilde{U}_0} = \frac{\tilde{F}}{S^2\tilde{u}_0} = (R_{\mathrm{R}} - iX_{\mathrm{R}})\frac{\rho c}{S}, \tag{77}$$

where $\tilde{U}_0$ is the total volume velocity produced by the disk and S is its surface area given by $S=\pi a^2$. R_{R} is the normalized radiation *resistance* given by

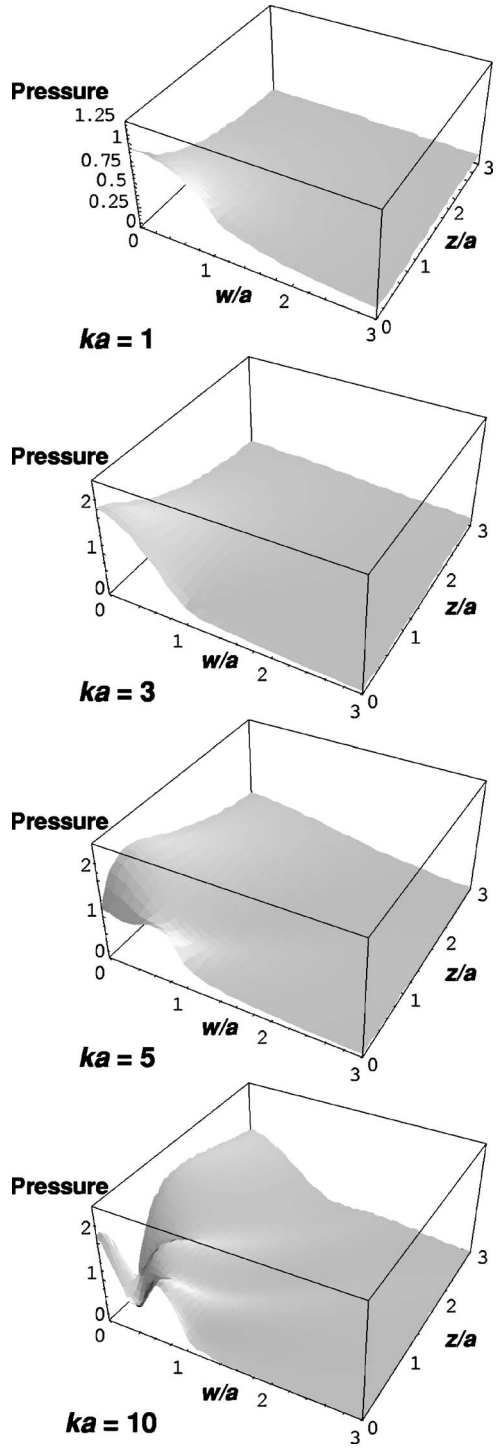

FIG. 9. Near-field pressure response of a disk in an infinite baffle.

$$R_{\mathrm{R}} = 1 - \frac{J_1(2ka)}{ka}, \tag{78}$$

and X_{R} is the normalized radiation *reactance* given by

$$X_{\mathrm{R}} = \frac{\mathbf{H}_1(2ka)}{ka}, \tag{79}$$

where J_1 is the first-order Bessel function and H_1 is the first-order Struve function. This result is plotted in Fig. 10. The following well-known asymptotic expressions can also be written:

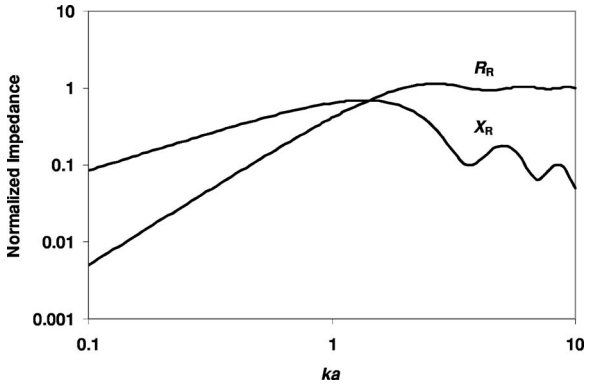

FIG. 10. Normalized radiation impedance of a disk in an infinite baffle.

$$R_{\mathrm{R}} \approx k^2a^2/2, \quad ka < 0.5, \tag{80}$$

$$X_{\mathrm{R}} \approx 8ka/(3\pi), \quad ka < 0.5. \tag{81}$$

D. Far-field response

Again, the first term or *monopole* part of the K-H boundary integral formula (1) is used, but this time in spherical coordinates

$$\tilde{p}(r,\theta,\phi) = 2\int_0^{2\pi}\int_0^a g\,(r,\theta,\phi|w_0,\phi_0,z_0)|_{z_0=0+} \times \frac{\partial}{\partial z_0}\,\tilde{p}(w_0,\phi_0,z_0)|_{z_0=0+} w_0\,dw_0\,d\phi_0. \tag{82}$$

Equation (62) and Eq. (72) can now be inserted into Eq. (82), again letting $n=0$ and $\phi=\pi/2$ so that $\cos(\phi-\phi_0)=\sin\phi_0$. Integrating over the surface of the disk while using Eq. (66) and Eq. (22) with $j_{0m}/b=k\sin\theta$ yields

$$\tilde{p}(r,\theta) = -ik\rho cS\tilde{u}_0\frac{1}{2\pi r}e^{-ikr}D(\theta), \tag{83}$$

where S is the area of the disk given by $S=\pi a^2$. The directivity function $D(\theta)$ is given by

$$D(\theta) = \frac{2J_1(ka\sin\theta)}{ka\sin\theta}. \tag{84}$$

The normalized directivity function $20\log_{10}|D(\theta)|$ is plotted in Fig. 11 for various values of ka. The on-axis pressure is evaluated using $\theta=0$ in Eq. (62) before inserting it into Eq. (82), which leads to

$$D(0) = 1. \tag{85}$$

The final result is most commonly written

$$\tilde{p}(r,0) = -i\omega\rho\tilde{U}_0\frac{1}{2\pi r}e^{-ikr}, \tag{86}$$

where the volume velocity is given by $\tilde{U}_0=S\tilde{u}_0$.

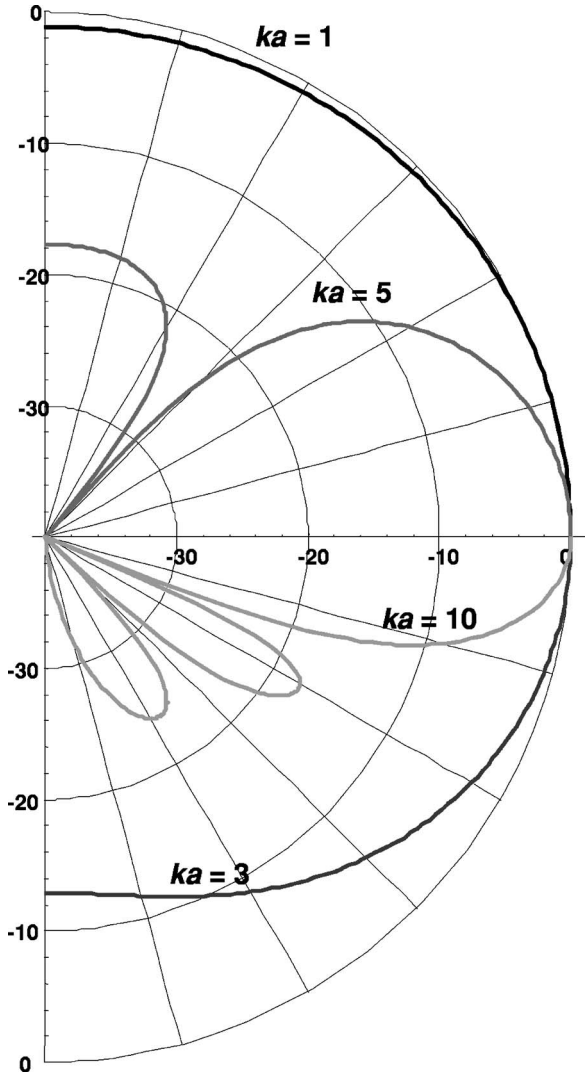

FIG. 11. Normalized far-field directivity function of a disk in an infinite baffle.

IV. RIGID DISK IN A FINITE, CLOSED-BACK CIRCULAR BAFFLE

A. Boundary conditions

The disk shown in Fig. 1, together with its circular baffle, lies in the xy plane and oscillates in the z direction with velocity $\tilde{u}_0$. The radius of the disk a and the inner and outer radii of the baffle are a and b, respectively. However, the configuration is now modified so that sound from the rear of the disk is blocked by a small cylindrical enclosure of radius b and depth h. The model is valid providing $h \leqslant a/4$, although the radiation impedance is virtually the same as that of a *rigid disk at the end of a flanged infinite tube* (or an unflanged tube[5] in the case of $b=a$). The area of each surface element is given by Eq. (2).

B. Near-field pressure

It is shown in Fig. 12 that the pressure distribution of the closed-back radiator is the sum of the outputs of the same radiator with an open back and in an infinite baffle. In other words, it uses the full K-H boundary integral of Eq. (1) including both the dipole and monopole parts. Hence, the near-field pressure distribution can be obtained by summing Eq. (61) and Eq. (75). However, in order to normalize the response, the resulting pressure is halved. The result is shown in Fig. 13 with $b=2a$ for various values of ka.

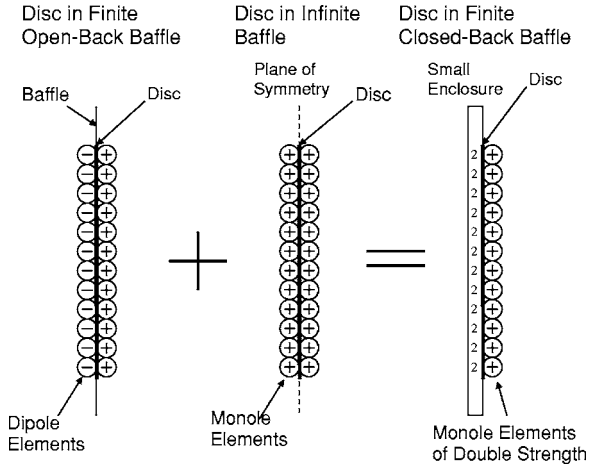

FIG. 12. Rigid disk in a finite closed-back circular baffle.

C. Radiation impedance

The same argument can be applied to the radiation impedance too, which is simply proportional to the sum of the surface pressures. The real part of the normalized radiation impedance can thus be obtained by combining Eq. (56) and Eq. (78) as follows:

$$R_{\mathrm{R}} = \frac{1}{2}\left(1 - \frac{J_1(2ka)}{ka} - kb\frac{b^2}{a^2}\sum_{m=0}^{M} \Re(\tau_m)\left\{1 - \left(1 - \frac{a^2}{b^2}\right)^{m+(3/2)}\right\}\right). \tag{87}$$

Similarly, the imaginary part can be obtained by combining Eq. (57) and Eq. (79)

$$X_{\mathrm{R}} = \frac{1}{2}\left(\frac{\mathbf{H}_1(2ka)}{ka} - kb\frac{b^2}{a^2}\sum_{m=0}^{M} \Im(\tau_m)\left\{1 - \left(1 - \frac{a^2}{b^2}\right)^{m+(3/2)}\right\}\right). \tag{88}$$

This result is plotted in Fig. 14. The asymptotic expressions can be written

$$R_{\mathrm{R}} \approx k^2a^2/4, \quad ka < 0.5, \tag{89}$$

$$X_{\mathrm{R}} \approx \frac{4}{\pi}\left(\frac{2b-a}{3b-a}\right)ka, \quad ka < 0.5. \tag{90}$$

D. Far-field response

The far-field response takes on the same form as that in both a finite open baffle given by Eq. (65) and an infinite baffle given by Eq. (83)

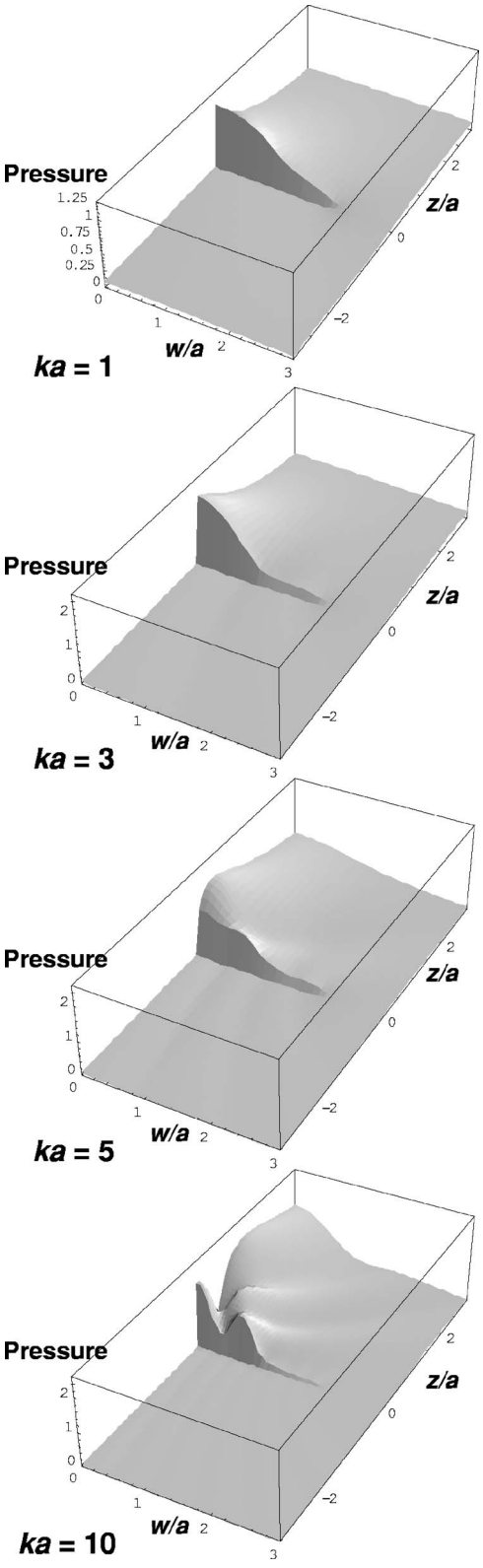

FIG. 13. Near-field pressure response of a disk in a finite closed-back baffle with $b=2a$.

$$\tilde{p}(r,\theta) = -ik\rho c S\tilde{u}_0 \frac{1}{2\pi r} e^{-ikr} D(\theta), \tag{91}$$

where S is the area of the disk given by $S=\pi a^2$. The directivity function $D(\theta)$ is obtained by combining the directivity function in a finite open baffle given by Eq. (67) with that in an infinite baffle given by Eq. (84)

$$D(\theta) = \frac{J_1(ka\sin\theta)}{ka\sin\theta} - kb\frac{b^2}{a^2}\cos\theta \sum_{m=0}^{M} \tau_m \Gamma\left(m+\frac{5}{2}\right) \times \left(\frac{2}{kb\sin\theta}\right)^{m+3/2} J_{m+(3/2)}(kb\sin\theta). \tag{92}$$

Similarly, the on-axis response may be obtained by combining the on-axis response in a finite open baffle given by Eq. (68) with that in an infinite baffle given by Eq. (85), where the latter is just unity

$$D(0) = \frac{1}{2}\left(1 - kb\frac{b^2}{a^2}\sum_{m=0}^{M}\tau_m\right). \tag{93}$$

The normalized on-axis response is shown in Fig. 15 again using Eq. (70). The normalized directivity function $20\log_{10}(|D(\theta)|/|D(0)|)$ is plotted in Fig. 16 with $b=2a$ for various values of ka and in Fig. 17 with $ka=\pi/2$ for various values of b/a.

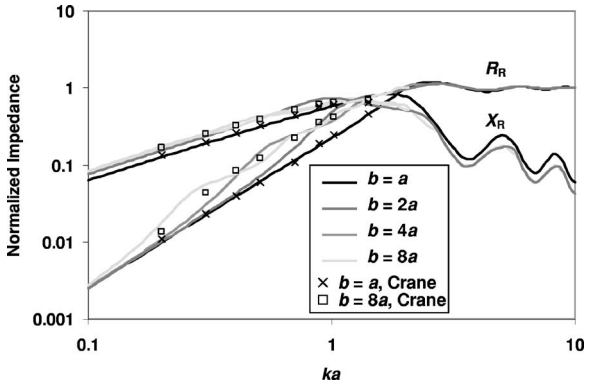

FIG. 14. Normalized radiation impedance of a disk in a finite closed-back baffle.

V. BABINET'S PRINCIPLE

Babinet's principle,[20] as developed by Bouwkamp[6] and Wiener,[4] states that the diffraction pattern resulting from the transmission of a plane wave through a hole in an infinite resilient screen (i.e., with zero surface impedance) is equivalent to that produced by the scattering of the same incident

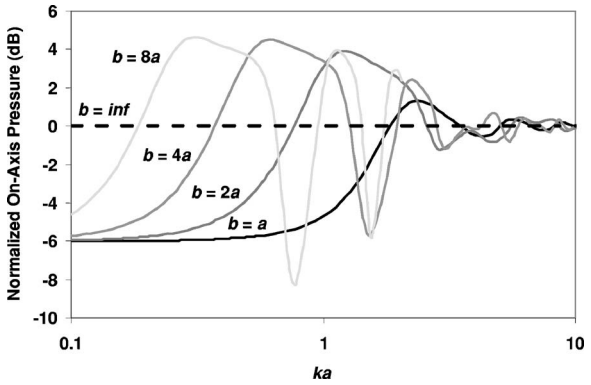

FIG. 15. Normalized far-field on-axis response of a disk in a finite closed-back baffle with constant acceleration.

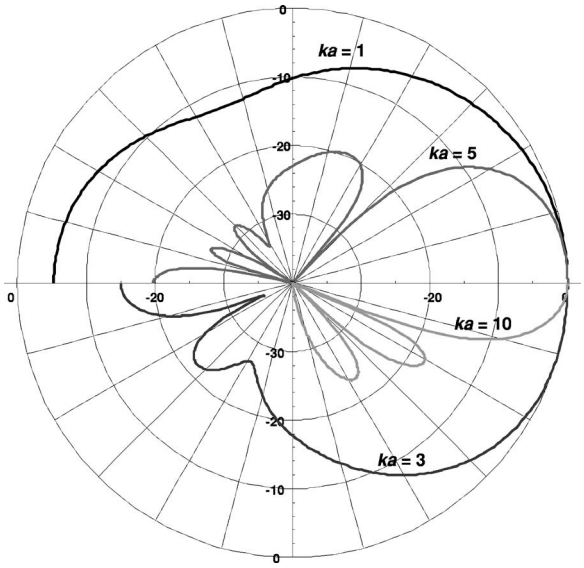

FIG. 16. Normalized directivity far-field function of a disk in a finite closed-back baffle with $b=2a$.

wave by the complementary rigid disk. Furthermore, the scattered wave is identical to that produced if the disk itself were oscillating in free space, providing the velocity of the disk is equal and opposite to the particle velocity of the incident wave at the surface of the disk or hole in the absence of any obstacle. This is illustrated in Fig. 18. For clarity, the diagram portrays the scattering of a sound wave at some very high frequency where there is minimal diffraction. However, the principle applies at all frequencies. The resulting sound field is given by

$$\tilde{p}(\mathbf{r}) = \tilde{p}_{\mathrm{Inc}}(\mathbf{r}) + \tilde{p}_{\mathrm{Scat}}(\mathbf{r}), \tag{94}$$

where $\tilde{p}_{\mathrm{Inc}}(\mathbf{r})$ is the incident sound field in the absence of a hole or disk given by

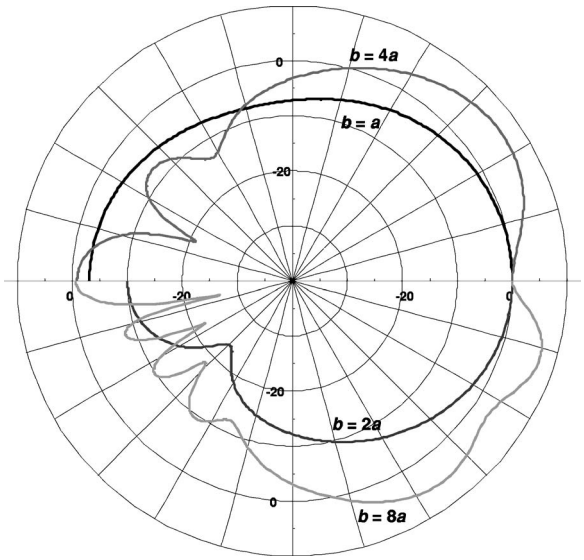

FIG. 17. Normalized directivity far-field function of a disk in a finite closed-back baffle with $ka=\pi/2$.

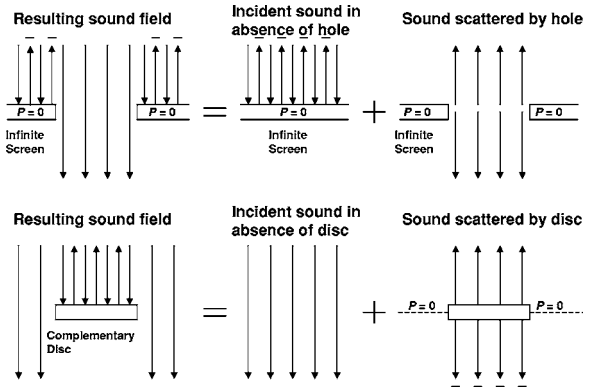

FIG. 18. Babinet's principle.

$$\tilde{p}_{\mathrm{Inc}}(z) = \begin{cases} -ik\rho c\tilde{\Psi}(e^{ikz} - e^{-ikz}), & \text{bright side of screen} \\ 0, & \text{dark side of screen} \\ -ik\rho c\tilde{\Psi}e^{ikz}, & \text{without disk(or screen)} \end{cases} \tag{95}$$

and using Eq. (75) for $\tilde{p}_{\mathrm{Scat}}(w,z)$ or Eqs. (83) and (84) for $\tilde{p}_{\mathrm{Scat}}(r,\theta)$. Also, it can be stated that the force $\tilde{F}_{\mathrm{inc}}$ exerted upon the disk by an incident wave is given by

$$\tilde{F}_{\mathrm{inc}} = z_{\mathrm{ar}} S \tilde{u}_{\mathrm{p}}, \tag{96}$$

where $\tilde{u}_{\mathrm{p}}$ is the undisturbed incident wave particle velocity at the surface of the disk and S is its surface area. The radiation impedance z_{ar} is given by Eqs. (55)–(57).

VI. APPROXIMATION FOR THE RIGID DISK IN FREE SPACE (RADIATION FROM AN UNBAFFLED RESILIENT DISK)

The following section contains a review of a historical approach to the problem of the disk in free space.[1] Prior to the work of Bouwkamp,[6] the Kirchhoff theory of diffraction had been used, which makes an assumption of equally distributed surface pressure in order to simplify the problem. In the case of diffraction, the pressure across the complementary hole in an infinite resilient screen is assumed to be the same as that of the incident wave, as if it were completely unaffected by the hole. In the case of radiation from a disk, if the pressure is constant, the velocity has to be allowed to vary across its radius so that it is no longer rigid. In fact, this produces a hypothetical sound source in which an equal driving force is applied directly to each air particle over the surface represented by the resilient "disk." Unlike a membrane, however, there is no boundary condition of zero displacement at the perimeter. Hence, this model creates some problems since it requires constant pressure to be maintained right up to the outer edge, where there is effectively an acoustic "short circuit" between the front and rear surfaces. Therefore, the reactive particle velocity at the perimeter is infinite, as is also the imaginary admittance.

The disk shown in Fig. 1 lies in the xy plane and a uniform driving force $\tilde{F}$ is applied in the z direction. The area of a surface element is given by Eq. (2) and the boundary

conditions of Eq. (3), Eq. (4), and Eq. (6) are assumed with $b=a$. Let the surface pressure distribution on the front and rear faces be defined by

$$\tilde{p}_+(w_0) = -\tilde{p}_-(w_0) = -\frac{\tilde{F}}{2S}, \tag{97}$$

where the total surface area S on each face is given by $S=\pi a^2$. Inserting Eq. (97) together with Eq. (14) in Eq. (8) and integrating over the surface area of the disk yields

$$\tilde{p}(w,z) = \frac{a\tilde{F}}{2S_D}\int_0^\infty J_1(\mu a)J_0(\mu w)e^{-i\sigma z}d\mu, \tag{98}$$

where Eq. (22) has been used. The disk velocity $\tilde{u}_0(w)$ can be derived from the boundary condition of Eq. (6) as follows:

$$\tilde{u}_0(w) = \frac{i}{k\rho c}\frac{\partial}{\partial z}\tilde{p}(w,z)|_{z=0+}$$

$$= \frac{a\tilde{F}}{2k\rho c S_D}\int_0^\infty J_1(\mu a)J_0(\mu w)\sigma\, d\mu. \tag{99}$$

Integrating the velocity over the area of the disk provides the total volume velocity $\tilde{U}_0$ as follows:

$$\tilde{U}_0 = \int_0^{2\pi}\int_0^a \tilde{u}_0(w)w\, dw\, d\phi = \frac{\pi a^2\tilde{F}}{k\rho c S_D}\int_0^\infty J_1^2(\mu a)\frac{\sigma}{\mu}d\mu, \tag{100}$$

where Eq. (22) has been used again. The acoustic radiation impedance z_{ar} can now be written as

$$z_{ar} = \frac{\tilde{F}}{S_D\tilde{U}_0} = \frac{2\rho c}{S_D Y_R}, \tag{101}$$

where Y_R is the normalized acoustic radiation *admittance*, which is expressed here as the sum of its real and imaginary parts

$$Y_R = G_R + iB_R, \tag{102}$$

where G_R is the normalized *conductance* given by

$$G_R = \frac{2}{k}\int_0^k \frac{\sqrt{k^2-\mu^2}}{\mu}J_1^2(\mu a)d\mu, \tag{103}$$

and B_R is the normalized *susceptance* given by

$$B_R = \frac{2}{k}\int_k^\infty \frac{\sqrt{\mu^2-k^2}}{\mu}J_1^2(\mu a)d\mu. \tag{104}$$

The solution[16] to Eq. (103) is

$$G_R = 1 + \frac{1}{ka}J_1(2ka) - 2J_0(2ka) - \pi[J_1(2ka)\mathbf{H}_0(2ka)$$

$$- J_0(2ka)\mathbf{H}_1(2ka)] \approx \frac{k^2a^2}{6}, \quad ka < 0.5. \tag{105}$$

Unfortunately, the integral in Eq. (104) does not converge and therefore cannot be solved due to the acoustic short circuit at the perimeter mentioned above. However, using the admittance of a disk in an infinite baffle from Sec. III and doubling it yields a reasonably good approximation to the actual solution for a rigid disk as follows:

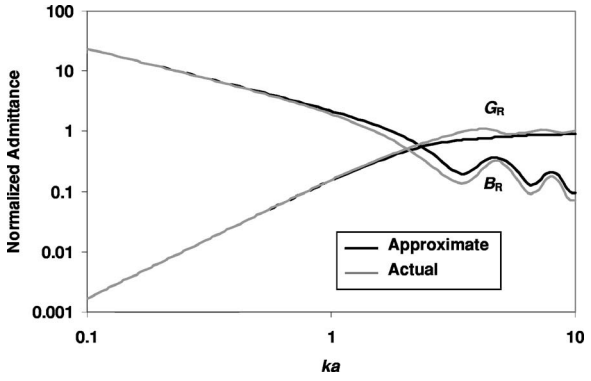

FIG. 19. Normalized radiation admittance of a disk in free space according to historical approximation.

$$B_R = \frac{2ka\mathbf{H}_1(2ka)}{[ka - J_1(2ka))^2 + (\mathbf{H}_1(2ka)]^2} \approx \frac{3\pi}{4ka}, \quad ka < 0.5. \tag{106}$$

The real and imaginary admittances G_R and B_R are plotted in Fig. 19 along with the actual admittances derived from Sec. II for comparison. Also, the impedance may be written as

$$R_R = \frac{G_R}{G_R^2 + B_R^2} \approx \frac{8k^4a^4}{27\pi^2}, \quad ka < 0.5, \tag{107}$$

$$X_R = \frac{B_R}{G_R^2 + B_R^2} \approx \frac{4ka}{3\pi}, \quad ka < 0.5. \tag{108}$$

Again, using Eq. (64) together with Eq. (97) and inserting them into Eq. (63) leads to the following directivity function:

$$D(\theta) = \frac{2J_1(ka\sin\theta)}{ka\sin\theta}\cos\theta. \tag{109}$$

VII. CONCLUSIONS

Referring to Fig. 5, it can be seen that in the case of an unbaffled rigid disk radiating from both sides, the on-axis sound output falls at 6 dB/octave for small values of ka due to the decreasing path difference (as a proportion of wavelength λ) between the antiphase rear radiation and the front radiation, which it partially cancels.

At larger values of ka, the rear radiation from the disk moves in and out of phase with that from the front. However, the comb filter effect is fairly "smeared," the largest peak being 3 dB at $ka=\pi/\sqrt{2}$ or $\lambda=2\sqrt{2}a$. The reason for this is that rear radiation comprises many point sources spread all across the radius of the disk, each with a different path length to the front, so that at no particular frequency do they produce a combined source that is either directly in phase or out of phase with the output from the front.

By contrast, when including a circular baffle and then increasing its size, the actual radiating area decreases in proportion to the total so that it behaves more like a coherent point source at the center. Hence, in the case of $b=4a$, a deep null can be seen at $ka=\pi/2$ or $\lambda=4a$, which is the distance

from the center to the edge. Of course, a disk at the center of a circular baffle is the "worst case," and it would be interesting to compare these results with those of an offset disk in a circular, rectangular, or elliptical baffle, for example, in order to "smear" the path difference effect. It could be postulated that, if the size of the baffle were increased still further, the response would converge towards that of an infinite baffle, where the latter is just a ruler flat line.

At larger values of ka, it can be seen that the near-field pressure responses in finite and infinite baffles converge (see Figs. 4 and 9, respectively). It seems that, as the polar response narrows, obstacles that are placed either side of the sound source have less effect upon the sound field. Also, distinct interference patterns start to emerge due to the presence of a rigid (i.e., opaque) sound source, or obstacle in the case of a scattered incident wave.

The on-axis response of the disk in a closed baffle, shown in Fig. 13, holds few surprises. As would be expected from the averaged response of a disk in a finite baffle and an infinite baffle, the same ripples as in Fig. 5 appear, but are reduced in magnitude. It is fairly well known that a source in a small enclosure produces 6 dB less sound output at low to medium frequencies in free space than when placed against a large plane surface. At high frequencies, of course, the size of the baffle has little effect and the source behaves as though the baffle is infinite. From the curves of Fig. 13, some idea may be gained of how the frequency at which the 6-dB shift occurs is related to the size of the baffle. In the impedance plot of Fig. 14, Crane's results for $b=a$ and $b=8a$ are included for comparison. In the case of $b=a$, the two calculation methods differ by less than 10%. However, when b is increased to $8a$, the real impedance differs by up to 24%, although the imaginary impedance matches within 5%.

Applying the unbaffled curve of Fig. 5 to the sound transmitted through a circular aperture (according to Babinet's principle), it can be seen that the hole is a weak radiator for small ka, as would be expected when considering that as the radiation impedance approaches zero, it increasingly matches that of the rest of the reflective screen. Even what little power does pass through the hole tends to flow back towards the screen. The power transmission coefficient is the real unbaffled impedance of Fig. 3. As Bouwkamp[6] and Spence[7] pointed out, a hole in a rigid screen is a much more effective radiator of power at low frequencies, returning an asymptotic transmission coefficient (or real radiation admittance) of $8/\pi^2$. The latter is a pressure source like the unbaffled resilient disk described in Sec. VI, where the pressure is that of the undisturbed incident wave and could therefore be considered as a resilient disk in an infinite baffle.

It can be seen from Fig. 17 that the approximation to the radiation admittance of a rigid disk in free space is surprisingly close to the actual solution and indeed converges towards it at low frequencies, yielding rational asymptotic expressions for the admittance and impedance. The main difference is that the ripples are missing from the real part at higher frequencies. The real part, however, is the rigorous transmission coefficient of the hypothetical resilient disk, and shows that such a transducer would be a much more effective radiator at low frequencies than a rigid disk, for which the transmission coefficient is the real impedance. However, the directivity function given by Eq. (109) is perhaps not such a useful approximation except at low frequencies ($ka \leqslant 3$). At high frequencies, it does not converge towards that of a disk in an infinite baffle, as does the actual directivity function of an unbaffled rigid disk.

Finally, when the surface velocity is expressed as a power series function of the radius, it is theoretically possible to accommodate any velocity distribution. This enables Eq. (17) for the velocity distribution to be applied to fluid-structure coupled problems, such as a circular membrane or plate, providing a suitable Green's function is used for the structure. In order to verify the method described in Sec. II, it has been found that Streng's results[14] can be reproduced, but only if the $m=0$ term of Eq. (7) is included. The reason originally stated for omitting this term[10] was that there is neither outward-radial nor axial particle displacement at the perimeter and therefore the radial pressure gradient there is expected to be zero. However, the radial particle displacement at the perimeter is due to the sum of the front and rear radial pressure gradients, which are equal and opposite and therefore cancel. The method has also been verified using FEM. It is hoped that the solutions provided in this paper serve as an illustration of how the symbolic handling capability of modern mathematical software tools may be used to simplify fundamental problems. For example, the conventional equations describing the radiation impedance of a rigid disk in free space or a finite open baffle were considered too complicated to reproduce in most textbooks, whereas Eqs. (47)–(51) and Eqs. (55)–(57) appear to be relatively compact.

ACKNOWLEDGMENT

The authors would like to express their gratitude to N. Lobo for his invaluable advice in numerical matters.

[1] P. M. Morse and K. U. Ingard, *Theoretical Acoustics* (McGraw-Hill, New York, 1968), pp. 320, 365, 389, 390.
[2] L. L. Beranek, *Acoustics* (Acoustical Society of America, New York, 1993), pp. 101–105, 118–128.
[3] H. F. Olson, *Acoustical Engineering* (Professional Audio Journals, Inc., Philadelphia, 1991), pp. 43–46, 92–99.
[4] F. M. Wiener, "On the relation between the sound fields radiated and diffracted by plane obstacles," J. Acoust. Soc. Am. **23**(6), 697–700 (1951).
[5] H. Levine and J. Schwinger, "On the radiation of sound from an unflanged circular pipe," Phys. Rev. **73**(4), 383–406 (1948).
[6] C. J. Bouwkamp, "Theoretical and numerical treatment of diffraction through a circular aperture," IEEE Trans. Antennas Propag. **AP18**(2), 152–176 (1970).
[7] R. D. Spence, "The diffraction of sound by circular disks and apertures," J. Acoust. Soc. Am. **20**(1), 380–386 (1948).
[8] J. Meixner and U. Fritze, "Das schallfeld in der nähe einer frei schwingenden kolbenmembran (The sound field in the vicinity of a freely oscillating piston diaphragm)," Z. Angew. Phys. **1**, 535–542 (1949).
[9] T. Nimura and Y. Watanabe, "Effect of a finite circular baffle board on acoustic radiation," J. Acoust. Soc. Am. **25**(1), 76–80 (1952).
[10] J. Pachner, "On the acoustical radiation of an emitter vibrating freely or in a wall of finite dimensions," J. Acoust. Soc. Am. **23**(2), 198–208 (1951).
[11] P. H. G. Crane, "Method for the calculation of the acoustic radiation impedance of unbaffled and partially baffled piston sources," J. Sound Vib. **5**(2), 257–277 (1967).
[12] T. J. Mellow, "On the mutual radiation characteristics of two rigid discs in open or closed finite circular baffles," *Joint Baltic–Nordic Acoustics Meet-*

ing 2004, 8–10 June 2004, Mariehamn, Åland, available online at the site ⟨http://www.acoustics.hut.fi/asf/bnam04/webprosari/onlineproc.html⟩
[13]J. H. Streng, "Calculation of the surface pressure on a vibrating circular stretched membrane in free space," J. Acoust. Soc. Am. **82**(2), 679–686 (1987).
[14]J. H. Streng, "Sound radiation from a circular stretched membrane in free space," J. Audio Eng. Soc. **37**(3), 107–118 (1989).
[15]I. S. Gradshteyn and I. M. Ryzhik, *Table of Integrals, Series, and Products*, 6th ed., edited by A. Jeffrey (Academic, New York, 2000), pp. 671, Eq. (6.567.1), pp. 668, Eq. (6.561.5), pp. 658, Eq. (6.521.1), pp. 900, Eq. (8.402), pp. 915, Eq. (8.465), pp. 902, Eq. (8.411.1).
[16]S. Wolfram, *The Mathematica Book*, 5th ed. (Wolfram Media, Champaign, Illinois, 2003).
[17]J. W. S. Rayleigh, *The Theory of Sound* (Dover, New York, 1945), Vol. II, pp. 107.
[18]H. Stenzel, "Über die berechnung des schallfeldes einer kreisförmigen kolbenmembran (On the calculation of the sound field of a circular piston diaphragm)," Elektrische Nachrichten-Technik **12**, 16–30 (1935).
[19]L. V. King, "On the acoustic radiation field of the piezoelectric oscillator and the effect of viscosity on the transmission," Can. J. Res. **11**, 135–146 (1934).
[20]J. Babinet, "Mémoires d'optique météorologique (Memoirs on meteorological optics)," C. R. Acad. Sci. Paris, **4**, 638 (1837).